Letter

Efficient method for quantum impurity problems out of equilibrium

Julian Thoenniss,* Michael Sonner,* Alessio Lerose, and Dmitry A. Abanin
Department of Theoretical Physics, University of Geneva, Quai Ernest-Ansermet 30, 1205 Geneva, Switzerland

(Received 24 November 2022; accepted 4 May 2023; published 23 May 2023)

We introduce an efficient method to simulate the dynamics of an interacting quantum impurity coupled to noninteracting fermionic reservoirs. Viewing the impurity as an open quantum system, we describe the reservoirs by their Feynman-Vernon influence functionals (IFs). The IFs are represented as matrix-product states in the temporal domain, which enables an efficient computation of the dynamics for arbitrary interactions. We apply our method to study quantum quenches and transport in an Anderson impurity model, including highly nonequilibrium setups, and find a favorable performance compared to state-of-the-art methods. The computational resources required for an accurate computation of the dynamics scale polynomially with evolution time, indicating that a broad class of out-of-equilibrium quantum impurity problems are efficiently solvable. This approach will provide additional insights into the dynamical properties of mesoscopic devices and correlated materials.

DOI: 10.1103/PhysRevB.107.L201115

Introduction. Nonequilibrium many-body dynamics is actively investigated in condensed matter and synthetic quantum systems such as ultracold atoms [1]. The aim of the ongoing quest is to find regimes where a nonequilibrium system exhibits desired physical properties, which may be qualitatively different compared to equilibrium. Theoretically, out-of-equilibrium many-body problems are extremely challenging, both for analytical and numerical methods [2,3].

Quantum impurity models (QIMs), where a small quantum system is coupled to reservoir(s) of itinerant electrons, naturally arise in a variety of systems, including mesoscopic conductors [4] and ultracold atoms [5,6]. Even simple QIMs such as the Anderson impurity model (AIM) [7] exhibit rich many-body physics including the Kondo effect whereby the impurity spin is screened by itinerant electrons [8]. Fermionic QIMs also play a central role in dynamical mean-field theory (DMFT), where the material properties are expressed via a self-consistent QIM [3,9].

A large number of methods for nonequilibrium QIMs have been developed in recent years. These include iterative path-integral approximations [10–12], non-Markovian [13,14] or auxiliary master equations (AMEs) [15,16], hierarchical equations of motion (HEOM) [17–19], time-dependent numerical renormalization group (NRG) [20–22] and density matrix renormalization group (tDMRG) [23–28], various variants of quantum Monte Carlo (QMC) [29–34], as well as variational [35,36] techniques. Recent advances including the inchworm algorithm [37] and increasingly sophisticated high-order diagrammatic calculations [38,39] ameliorated the sign problem of QMC, thereby giving access to longer evolution times. However, the current methods cannot provide guarantees of computational efficiency for out-of-equilibrium QIMs, which remain a subject of active research.

Here, we present a nonperturbative approach for fermionic QIMs with efficiency guarantees; a companion paper [40] provides additional technical background. Our approach uses insights from recent developments in describing interacting quantum baths [41–52] and free bosonic environments [53,54] but the methodology and field of applicability differ significantly. We treat the impurity as an open quantum system coupled to the "bath" that consists of fermionic leads (Fig. 1). Their effect is represented by the fermionic Feynman-Vernon influence functional (IF) [55] which is obtained in closed form for arbitrary bath geometry [3,14,40]. As a key ingredient of our approach, the IF can be efficiently represented as a matrix-product state (MPS) in the temporal domain with controlled bond dimension, owing to the favorable scaling of temporal entanglement [40,44]. This enables an efficient computation of time-dependent observables at the impurity location (e.g., charge, spin, currents) via straightforward tensor contraction.

We demonstrate the efficiency of our method for paradigmatic nonequilibrium QIM setups, including (i) a quantum quench, where an impurity site is connected to equilibrium leads at time $t = 0$, and (ii) a biased AIM with two imbalanced leads. In all cases, our method is capable of reproducing and going beyond the state-of-the-art results obtained by inchworm and diagrammatic QMC.

Besides conceptual simplicity, the method presented here has a number of advantages. First, computational complexity grows only polynomially with evolution time, implying that QIMs are efficiently solvable even out of equilibrium [56,57]. Furthermore, the method is nonperturbative, in contrast, e.g., to QMC, which involves perturbative expansions either in the impurity-reservoir hybridization or in the on-site Coulomb interaction. In addition, once an efficient MPS representation of the reservoirs' IF is found, the dynamics of impurities with an arbitrary choice of time-dependent local Hamiltonian can be computed with modest effort.

*These authors contributed equally to this work.

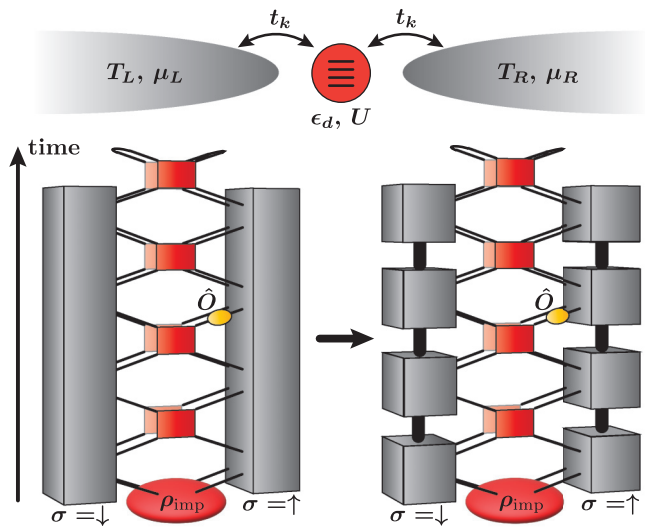

FIG. 1. Top: Illustration of a single-impurity Anderson model [Eq. (1)] with an impurity (red) tunnel-coupled to two reservoirs (gray). Bottom: Tensor-network representation of a time-dependent observable $\langle\hat{O}(t)\rangle$. The dynamical influence of the environment is encoded in one IF per orbital (here, two gray tensors for $\sigma=\uparrow,\downarrow$, left) which can be efficiently represented as MPS in the temporal domain (right) and hence contracted with the local impurity evolution (product of red tensors). The foreground (background) layer represents the forward (backward) branch of the Keldysh contour.

Description of the method. We consider the single-impurity Anderson model, described by the Hamiltonian

$$H=\sum_{\substack{k\\ \sigma=\uparrow,\downarrow\\ \alpha=L,R}}[(t_k d_\sigma^\dagger c_{k,\alpha,\sigma}+\text{H.c.})+\epsilon_k c_{k,\alpha,\sigma}^\dagger c_{k,\alpha,\sigma}]+H_{\rm imp}, \quad (1)$$

with $H_{\rm imp}=(\epsilon_d-U/2)\sum_\sigma \hat{d}_\sigma^\dagger\hat{d}_\sigma+U\hat{d}_\uparrow^\dagger\hat{d}_\uparrow\hat{d}_\downarrow^\dagger\hat{d}_\downarrow$. The impurity level described by fermions d_σ is coupled to two baths ($\alpha=L,R$) of free fermions $c_{k,\alpha,\sigma}$ with identical dispersion ϵ_k and tunnel couplings t_k, initially in thermal equilibrium (see the top illustration in Fig. 1). The Coulomb interaction $U\neq 0$ in $H_{\rm imp}$ gives rise to strong correlations. We are primarily interested in the real-time evolution of an impurity observable $\langle\hat{O}(t)\rangle$ starting from a factorized initial state $\rho(0)=\rho_L\otimes\rho_{\rm imp}\otimes\rho_R$, with $\rho_{L,R}$ equilibrium states at inverse temperatures $\beta_{L,R}$ and chemical potentials $\mu_{L,R}$. While conventional tensor-network approaches attempt to compactly represent $\rho(t)$ [2], we instead express $\langle\hat{O}(t)\rangle$ as a Keldysh path integral over Grassmann trajectories of impurity and baths. Gaussian integration over the bath trajectories gives

$$\begin{aligned}\langle\hat{O}(t)\rangle\propto&\int\left(\prod_{\sigma,\tau}d\bar{\eta}_{\sigma,\tau}d\eta_{\sigma,\tau}\right)\mathcal{O}(\bar{\boldsymbol{\eta}}_t,\boldsymbol{\eta}_t)\\&\times\exp\left\{\int_{\mathcal{C}}d\tau\left[\sum_\sigma\bar{\eta}_{\sigma,\tau}\partial_\tau\eta_{\sigma,\tau}-i\mathcal{H}_{\rm imp}(\bar{\boldsymbol{\eta}}_\tau,\boldsymbol{\eta}_\tau)\right]\right\}\\&\times\rho_{\rm imp}[\bar{\boldsymbol{\eta}}_0,\boldsymbol{\eta}_0]\prod_{\sigma=\uparrow,\downarrow}\\&\times\exp\left(\int_{\mathcal{C}}d\tau\int_{\mathcal{C}}d\tau'\bar{\eta}_{\sigma,\tau}\Delta(\tau,\tau')\eta_{\sigma,\tau'}\right).\end{aligned} \quad (2)$$

Here, $\bar{\boldsymbol{\eta}}_\tau=(\bar{\eta}_{\uparrow,\tau},\bar{\eta}_{\downarrow,\tau})$ and $\boldsymbol{\eta}_\tau=(\eta_{\uparrow,\tau},\eta_{\downarrow,\tau})$ parametrize the impurity trajectory. The IF is the last exponential in Eq. (2), defined by the hybridization function $\Delta(\tau,\tau')=\sum_\alpha\Delta^\alpha(\tau,\tau')$, where Δ^α fully encodes the dynamical influence of the bath α,

$$\Delta^\alpha(\tau,\tau')=\int\frac{d\omega}{2\pi}\Gamma(\omega)g^\alpha_{\tau,\tau'}(\omega). \quad (3)$$

The latter is determined by the bath's spectral density $\Gamma(\omega)=2\pi\sum_k|t_k|^2\delta(\omega-\epsilon_k)$ and noninteracting Green's function $g^\alpha_{\tau,\tau'}(\omega)=[n^\alpha_{\rm F}(\omega)-\Theta_{\mathcal{C}}(\tau,\tau')]e^{-i\omega(\tau-\tau')}$, where $n^\alpha_{\rm F}$ is the Fermi distribution at inverse temperature β_α and chemical potential μ_α and $\Theta_{\mathcal{C}}$ is the Heaviside step function on the Keldysh contour $\mathcal{C}$ (see, e.g., Ref. [3]). Equation (2) is the starting point of advanced techniques such as AME, HEOM, or QMC.

The difficulty in evaluating the path integral arises from the combination of non-Gaussianity (in $\mathcal{H}_{\rm imp}$) and time nonlocality [in $\Delta(\tau,\tau')$]. In our approach, we interpret Eq. (2) as a scalar product of fictitious states and operators defined in a fermionic Fock space on a temporal lattice. We note that the textbook expression in Eq. (2) is defined as the limit $M\to\infty$ of a discrete-time expression, obtained by dividing the full time evolution window $[0,T]$ into M steps of size $\delta t=T/M$; we fix a sufficiently large M. It is convenient to use a Trotter scheme that further splits the Trotter step into impurity and hybridization, leading to $8M$ variables per spin species along the Keldysh contour [see Supplemental Material (SM) [58]]. We arrange these in two arrays, $\boldsymbol{\eta}_\sigma=(\eta_{\sigma,0^+},\eta_{\sigma,0^-},\ldots,\eta_{\sigma,(2M-1)^+},\eta_{\sigma,(2M-1)^-})$ and analogously $\bar{\boldsymbol{\eta}}_\sigma$, with degrees of freedom alternating on the forward (+) and backward (−) branch of the Keldysh contour. A series of manipulations with the discrete-time path integral [59] allows us to rewrite Eq. (2) as a scalar product (see SM [58]):

$$\begin{aligned}\langle\hat{O}(t)\rangle\propto&\int\left(\prod_\sigma d\bar{\boldsymbol{\eta}}_\sigma d\boldsymbol{\eta}_\sigma\right)\\&\times\mathcal{I}[\boldsymbol{\eta}_\downarrow]e^{-\bar{\boldsymbol{\eta}}_\downarrow\boldsymbol{\eta}_\downarrow}\mathcal{D}_{\mathcal{O},t}[\bar{\boldsymbol{\eta}}_\downarrow,\boldsymbol{\eta}_\uparrow]e^{-\bar{\boldsymbol{\eta}}_\uparrow\boldsymbol{\eta}_\uparrow}\mathcal{I}[\bar{\boldsymbol{\eta}}_\uparrow]\\\equiv&\langle I|\,\hat{D}_{\hat{O},t}\,|I\rangle\,.\end{aligned} \quad (4)$$

Here, the non-Gaussian kernel $\mathcal{D}_{\mathcal{O},t}[\bar{\boldsymbol{\eta}}_\downarrow,\boldsymbol{\eta}_\uparrow]$ describes the impurity's own dynamics and is local in time. This gives rise to a product operator $\hat{D}_{\hat{O},t}=\hat{D}_1\otimes\cdots\otimes\hat{D}_M$, where each $\hat{D}_m$ is a 16×16 matrix (except the first and last; see superimposed red tensors in Fig. 1) and $\hat{D}_{m^*=t/\delta t}$ contains $\hat{O}$. The discrete-time IF has a Gaussian form, $\mathcal{I}[\boldsymbol{\eta}_\sigma]=\exp(\boldsymbol{\eta}_\sigma^T\mathbf{B}\,\boldsymbol{\eta}_\sigma)$, where the antisymmetric matrix $\mathbf{B}$ is related to the time discretization of $\Delta(\tau,\tau')$ (see SM [58]). The Gaussian many-body wave function $|I\rangle$ associated with $\mathcal{I}$ (gray tensors in Fig. 1, bottom left) is obtained by replacing Grassmann variables by corresponding creation operators acting on the Fock space vacuum, $\mathbf{c}^\dagger\equiv(c^\dagger_{0^+},c^\dagger_{0^-},\ldots,c^\dagger_{(2M-1)^+},c^\dagger_{(2M-1)^-})$,

$$|I\rangle=\exp(\mathbf{c}^{\dagger T}\mathbf{B}\,\mathbf{c}^\dagger)\,|\emptyset\rangle\,. \quad (5)$$

Such a state formally has a Bardeen-Cooper-Schrieffer form, regardless of the fermion-number conservation of the original problem [cf. Eq. (2)]. We note that particle number conservation shows up as a sublattice symmetry in Eq. (5).

Next, we aim to represent the state $|I\rangle$ as a MPS. Correlations of this state reflect non-Markovianity of the bath. The possibility of a compact MPS representation is determined by the entanglement properties of a wave function; in Ref. [40] we show that Gaussian IF wave functions arising in QIM exhibit at most logarithmic scaling of temporal entanglement with evolution time for both equilibrium and certain nonequilibrium initial states of the reservoirs. This suggests that such wave functions can be described by a polynomial-in-T number of parameters.

Previous works [60,61] proposed algorithms for representing a fermionic Gaussian wave function as a MPS. Here, we apply the Fishman-White (FW) algorithm [60], extended to BCS-like wave functions [40]. We first approximately represent the Gaussian state determined by **B** [Eq. (5)] as a quantum circuit of nearest-neighbor Gaussian unitary gates applied to the vacuum. The approximation is controlled by a threshold parameter ϵ of the algorithm [40,60], which determines the maximum number D of gates acting on a given site in this circuit (the "local depth"). Second, we compress the circuit with standard singular-value truncations to produce a MPS approximation of $|I\rangle$ with bond dimension $\chi \leqslant 2^D$. Once the MPS is obtained (gray tensors in Fig. 1, bottom right), the impurity's reduced density matrix time evolved with an arbitrary (possibly time-dependent) impurity Hamiltonian $H_{\rm imp}$ can be efficiently computed by tensor contraction in the time direction. This method is straightforwardly applicable to the computation of multitime observables, e.g., the impurity Green's function, as well as currents (see below).

A quantum quench. As a first application of our method, we study a local quantum quench, where tunneling between impurity and the bath—initially in equilibrium at equal β and μ—is turned on at time $t = 0$. We monitor the real-time evolution of the impurity level population at $t > 0$. In the Kondo regime (strong interaction and low temperature), strong correlations develop in real time between the impurity and the bath, corresponding to the formation of a local screening cloud over a nonperturbatively long timescale [20,21,24,35,62].

Here, we benchmark the state-of-the-art results of inchworm QMC in Ref. [37]: We consider a bath defined by a flat band with smooth edges, $\Gamma(\omega) = \Gamma/[(1 + e^{\nu(\omega-\omega_c)})(1 + e^{-\nu(\omega+\omega_c)})]$ with $\omega_c = 10\Gamma$ and $\nu = 10/\Gamma$. Moreover, we set $\beta = 50/\Gamma$, $\mu = 0$. We prepare the impurity in a singly occupied state $\rho_{\rm imp} = |\uparrow\rangle\langle\uparrow|$, with $\epsilon_d = 0$ and $U = 8\Gamma$, and couple it to the bath at time $t = 0$. In Fig. 2 we report our results for the evolution of the diagonal components of the impurity's reduced density matrix. Data are converged with respect to all simulation parameters (see the caption), demonstrating accuracy beyond the data of Ref. [37]. These results showcase the ability of our method to capture the slow dynamical formation of a spin singlet in the Kondo regime, which will be further investigated elsewhere.

Nonequilibrium transport. The system described by Eq. (1) with a temperature or chemical potential bias between the L and R reservoirs models paradigmatic nonequilibrium setups with correlated nanodevices. Capturing the full transient charge and spin dynamics after a quench toward the nonequilibrium stationary state is a recurrent challenging test for novel advanced numerical techniques [22,38,63–65].

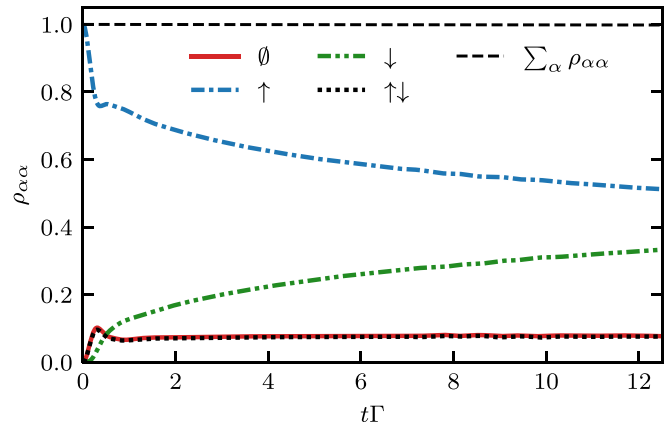

FIG. 2. Real-time evolution of the impurity density matrix after a quench. The plot reports diagonal entries $\rho_{\alpha\alpha}$, with $\alpha = \emptyset, \uparrow, \downarrow, \uparrow\downarrow$ as a function of time. The environment is modeled as in Ref. [37] (see main text), with $\beta = 50/\Gamma$ and $\mu = 0$. Simulation parameters: Bond dimension $\chi = 256$ per spin species, FW threshold $\epsilon = 5 \times 10^{-13}$, Trotter step $\delta t = 0.02/\Gamma$.

Here, we benchmark the state-of-the-art computation of the system's current-voltage characteristics in Ref. [38]. We model the reservoirs as two homogeneous tight-binding chains with nearest-neighbor hopping $t_{\rm hop} = 1$, coupled to the impurity with tunneling amplitude $t'_{\rm hop} = 0.3162$, corresponding to a resonance width $\Gamma(\epsilon_d = 0) = 0.1$ (cf. Ref. [24]). We initialize the two reservoirs at zero temperature and chemical potentials $\pm V/2$, and monitor the time-dependent current flowing through the impurity for several values of U, until the stationary state is reached.

Unlike the contraction illustrated in Fig. 1 and used above for the quench simulation, computing the current into either reservoir requires one to keep track of the separate influence of reservoirs L and R. A suitable Trotter decomposition (see Ref. [40] and SM [58]) allows us to couple the two reservoirs with the impurity alternatively in discrete time steps δt. The current of spin σ electrons flowing into reservoir α can then be computed as $\langle I_{\alpha,\sigma}(t)\rangle = \frac{1}{\delta t}[\langle d^\dagger_\sigma(t+\delta t) d_\sigma(t+\delta t)\rangle - \langle d^\dagger_\sigma(t) d_\sigma(t)\rangle]$, where the impurity interacts only with reservoir α during the time step from t to $t + \delta t$.

Keeping track of L and R separately results in a tensor contraction with four IF MPS. This considerably limits the bond dimension we can afford for each IF, as the final impurity evolution entails storing matrices acting on a $16\chi^4$-dimensional space (while it was $16\chi^2$ before). Nonetheless, we found that the value of the current is converged over the full transient to the stationary state for bond dimension as low as $\chi = 32$ (see the inset of Fig. 3).

Figure 3 shows the results of our computations, as well as the corresponding data from Fig. 15 of Ref. [38]. We find a fairly good agreement throughout the wide explored parameter regime. The unit slope of the dotted line represents the universal Landauer linear-response conductance, $I = (e^2/h)V$ (recall $e = \hbar = 1$ in our units). We note that small discrepancies are to be expected at large biases $V \gg \Gamma$ due to the nonuniversal effects of the finite bath bandwidth ($t_{\rm hop} = 10\Gamma$ here). We further remark that for small bias and large interaction the nonequilibrium Kondo regime is approached,

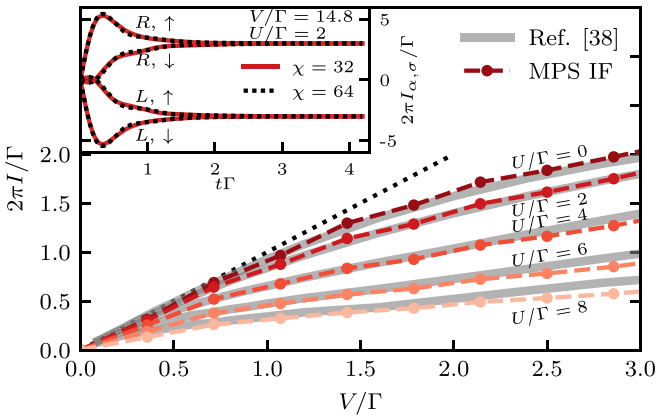

FIG. 3. Current-voltage characteristics of an AIM. Reservoirs L and R are tight-binding chains as in Refs. [24,38] (see the main text), of $L = 600$ sites each, at zero temperature and chemical potentials $\pm V/2$. Simulation parameters: Bond dimension $\chi = 32$ per reservoir per spin species, FW threshold $\epsilon = 1 \times 10^{-12}$, Trotter step $\delta t = 0.007/\Gamma$. For all values of V and U we evolve until time $T = 4.2/\Gamma$ and verify that at this time a stationary state is reached. Inset: At fixed $V/\Gamma = 14.8$ and $U/\Gamma = 2$, we demonstrate convergence in bond dimension for all four components of the transient current, $\langle I_{\alpha,\sigma}(t)\rangle$ with $\alpha = L, R$ and $\sigma = \uparrow, \downarrow$.

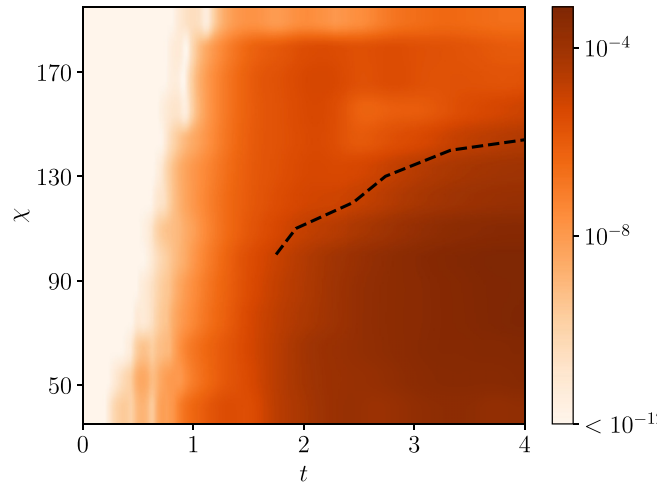

FIG. 4. Error $e(t, \chi)$ of the time-evolved impurity density matrix as a function of bond dimension and evolution time (see the main text), for an impurity starting from $\rho_{\text{imp}}(0) = |\uparrow\rangle\langle\uparrow|$ and coupled with tunneling amplitude $t'_{\text{hop}} = 0.3162$ to a single tight-binding chain of $L = 400$ sites with homogeneous nearest-neighbor hopping $t_{\text{hop}} = 1$, initially at zero temperature and half filling (cf. Ref. [24]). The constant-error $e = 10^{-5}$ dashed line indicates that the required bond dimension grows slowly with simulation time. Here, we fixed $T = 4$, $\delta t = 0.01$, $\epsilon = 10^{-12}$.

characterized by slow relaxation. Accordingly, in the computation with the smallest bias $V = 0.36\Gamma$ and largest interaction $U = 8\Gamma$ in Fig. 3, the time-dependent current has not yet fully reached its stationary value at time T.

Computational efficiency. Finally, we report on the computational efficiency of our method. Previous works found that for Gaussian ground states [60] and IFs [40], the FW algorithm produces a quantum circuit of "local depth" $D = D(T)$ that scales at most logarithmically with evolution time T. We note that the FW control parameter ϵ affects the prefactor of $\log T$ scaling of D. In turn, D puts an exact upper bound on the bond dimension of the corresponding MPS as $\chi \leqslant 2^D$ [40,60], indicating that the computational complexity of the algorithm scales at most polynomially with evolution time.

We found that compression of the FW circuit using conventional singular-value truncation typically leads to a further significant reduction of the required computational resources. For the data shown in Fig. 2, we find a maximum "local depth" $D = 28$ which sets the hard upper bound $\chi \leqslant 2^{28}$. However, this circuit could be accurately approximated by a MPS with a much smaller bond dimension $\chi = 256 = 2^8$.

In order to assess the *a posteriori* error of observables due to MPS compression, we considered an environment that consists of a single tight-binding chain [66]. Having fixed an extremely low FW threshold ϵ (which makes this source of error negligible), we estimated the residual error of time-dependent observables in $t \in [0, T]$ due to the truncated bond dimension, as the trace distance $e(t, \chi) = ||\rho^{(\chi)}_{\text{imp}}(t) - \rho^{(\infty)}_{\text{imp}}(t)||_1$ between the reduced density matrix computed with a cutoff χ on the IF MPS and the fully converged result (computed using a much higher $\chi = 512$).

The behavior of the error e as a function of t and χ is illustrated in Fig. 4. We observe that the bond dimension $\chi = \chi(t)$ required to achieve a fixed error e grows approximately linearly with t, indicating the efficiency of the approach. We similarly found in other cases that a moderate bond dimension is sufficient to accurately compute impurity observables. Thus, we conclude that our approach indeed has polynomial complexity [40,44], allowing one to access long-time impurity dynamics with present-day computational resources.

Summary and outlook. To summarize, we introduced a method for studying dynamics of QIM, based on a tensor-network representation of the reservoir's IF. We applied this approach to paradigmatic quantum quenches in AIM, demonstrating that it compares favorably to state-of-the art QMC computations. The approach is nonperturbative and offers several other advantages: In particular, it applies to both equilibrium and highly nonequilibrium QIM setups. Moreover, once a MPS form of the IF is obtained, arbitrary choices of impurity interactions can be analyzed with modest extra effort.

We showed that the required computational resources scale polynomially with the evolution time, suggesting the efficiency of our approach for a broad range of QIM problems. The approach can straightforwardly be extended to different setups, including multiorbital impurities and initial states with entanglement between impurity and reservoirs. Another promising application is to DMFT, which will require an imaginary-time extension of the technique introduced here. We expect the computational efficiency of the approach to enable long-time simulations of dynamics in such setups as well, opening the door to analyzing nonequilibrium behavior of mesoscopic devices and quantum materials.

Note added. Recently, we became aware of a related work by Ng *et al.* [67].

Data relating to this article is archived in YARETA [68].

Acknowledgments. We thank E. Arrigoni, G. Cohen, M. Eckstein, S. Florens, Y. Ke, M. Stoudenmire, and X. Waintal

for discussions. Support by the European Research Council (ERC) under the European Union's Horizon 2020 research and innovation programme (Grant Agreement No. 864597) and by the Swiss National Science Foundation is gratefully acknowledged.

[1] I. Bloch, J. Dalibard, and W. Zwerger, Many-body physics with ultracold gases, Rev. Mod. Phys. **80**, 885 (2008).
[2] S. Paeckel, T. Köhler, A. Swoboda, S. R. Manmana, U. Schollwöck, and C. Hubig, Time-evolution methods for matrix-product states, Ann. Phys. **411**, 167998 (2019).
[3] H. Aoki, N. Tsuji, M. Eckstein, M. Kollar, T. Oka, and P. Werner, Nonequilibrium dynamical mean-field theory and its applications, Rev. Mod. Phys. **86**, 779 (2014).
[4] M. Pustilnik and L. Glazman, Kondo effect in quantum dots, J. Phys.: Condens. Matter **16**, R513 (2004).
[5] M. Kanász-Nagy, Y. Ashida, T. Shi, C. P. Moca, T. N. Ikeda, S. Fölling, J. I. Cirac, G. Zaránd, and E. A. Demler, Exploring the anisotropic Kondo model in and out of equilibrium with alkaline-earth atoms, Phys. Rev. B **97**, 155156 (2018).
[6] L. Riegger, N. Darkwah Oppong, M. Höfer, D. R. Fernandes, I. Bloch, and S. Fölling, Localized Magnetic Moments with Tunable Spin Exchange in a Gas of Ultracold Fermions, Phys. Rev. Lett. **120**, 143601 (2018).
[7] P. W. Anderson, Localized magnetic states in metals, Phys. Rev. **124**, 41 (1961).
[8] A. C. Hewson, *The Kondo Problem to Heavy Fermions*, Cambridge Studies in Magnetism (Cambridge University Press, Cambridge, UK, 1993).
[9] A. Georges, G. Kotliar, W. Krauth, and M. J. Rozenberg, Dynamical mean-field theory of strongly correlated fermion systems and the limit of infinite dimensions, Rev. Mod. Phys. **68**, 13 (1996).
[10] D. E. Makarov and N. Makri, Path integrals for dissipative systems by tensor multiplication. Condensed phase quantum dynamics for arbitrarily long time, Chem. Phys. Lett. **221**, 482 (1994).
[11] S. Weiss, J. Eckel, M. Thorwart, and R. Egger, Iterative real-time path integral approach to nonequilibrium quantum transport, Phys. Rev. B **77**, 195316 (2008).
[12] D. Segal, A. J. Millis, and D. R. Reichman, Numerically exact path-integral simulation of nonequilibrium quantum transport and dissipation, Phys. Rev. B **82**, 205323 (2010).
[13] M. W. Y. Tu and W.-M. Zhang, Non-Markovian decoherence theory for a double-dot charge qubit, Phys. Rev. B **78**, 235311 (2008).
[14] J. Jin, M. Wei-Yuan Tu, W.-M. Zhang, and Y. Yan, Non-equilibrium quantum theory for nanodevices based on the Feynman-Vernon influence functional, New J. Phys. **12**, 083013 (2010).
[15] A. Dorda, M. Nuss, W. von der Linden, and E. Arrigoni, Auxiliary master equation approach to nonequilibrium correlated impurities, Phys. Rev. B **89**, 165105 (2014).
[16] M. Lotem, A. Weichselbaum, J. von Delft, and M. Goldstein, Renormalized Lindblad driving: A numerically exact nonequilibrium quantum impurity solver, Phys. Rev. Res. **2**, 043052 (2020).
[17] Y. Tanimura and R. Kubo, Time evolution of a quantum system in contact with a nearly Gaussian-Markoffian noise bath, J. Phys. Soc. Jpn. **58**, 101 (1989).
[18] J. Jin, X. Zheng, and Y. Yan, Exact dynamics of dissipative electronic systems and quantum transport: Hierarchical equations of motion approach, J. Chem. Phys. **128**, 234703 (2008).
[19] X. Dan, J. T. Xu, Meng Stockburger, J. Ankerhold, and Q. Shi, Efficient low temperature simulations for fermionic reservoirs with the hierarchical equations of motion method: Application to the Anderson impurity model, arXiv:2211.04089 [Phys. Rev. B (to be published)].
[20] F. B. Anders and A. Schiller, Real-Time Dynamics in Quantum-Impurity Systems: A Time-Dependent Numerical Renormalization-Group Approach, Phys. Rev. Lett. **95**, 196801 (2005).
[21] H. T. M. Nghiem and T. A. Costi, Time Evolution of the Kondo Resonance in Response to a Quench, Phys. Rev. Lett. **119**, 156601 (2017).
[22] F. Schwarz, I. Weymann, J. von Delft, and A. Weichselbaum, Nonequilibrium Steady-State Transport in Quantum Impurity Models: A Thermofield and Quantum Quench Approach Using Matrix Product States, Phys. Rev. Lett. **121**, 137702 (2018).
[23] J. Prior, A. W. Chin, S. F. Huelga, and M. B. Plenio, Efficient Simulation of Strong System-Environment Interactions, Phys. Rev. Lett. **105**, 050404 (2010).
[24] M. Nuss, M. Ganahl, E. Arrigoni, W. von der Linden, and H. G. Evertz, Nonequilibrium spatiotemporal formation of the Kondo screening cloud on a lattice, Phys. Rev. B **91**, 085127 (2015).
[25] F. A. Wolf, I. P. McCulloch, and U. Schollwöck, Solving nonequilibrium dynamical mean-field theory using matrix product states, Phys. Rev. B **90**, 235131 (2014).
[26] A. Nüßeler, I. Dhand, S. F. Huelga, and M. B. Plenio, Efficient simulation of open quantum systems coupled to a fermionic bath, Phys. Rev. B **101**, 155134 (2020).
[27] G. Wójtowicz, J. E. Elenewski, M. M. Rams, and M. Zwolak, Open-system tensor networks and Kramers' crossover for quantum transport, Phys. Rev. A **101**, 050301(R) (2020).
[28] L. Kohn and G. E. Santoro, Quench dynamics of the anderson impurity model at finite temperature using matrix product states: Entanglement and bath dynamics, J. Stat. Mech. (2022) 063102.
[29] L. Mühlbacher and E. Rabani, Real-Time Path Integral Approach to Nonequilibrium Many-Body Quantum Systems, Phys. Rev. Lett. **100**, 176403 (2008).
[30] M. Schiró and M. Fabrizio, Real-time diagrammatic Monte Carlo for nonequilibrium quantum transport, Phys. Rev. B **79**, 153302 (2009).
[31] P. Werner, T. Oka, and A. J. Millis, Diagrammatic Monte Carlo simulation of nonequilibrium systems, Phys. Rev. B **79**, 035320 (2009).
[32] E. Gull, D. R. Reichman, and A. J. Millis, Numerically exact long-time behavior of nonequilibrium quantum impurity models, Phys. Rev. B **84**, 085134 (2011).
[33] G. Cohen and E. Rabani, Memory effects in nonequilibrium quantum impurity models, Phys. Rev. B **84**, 075150 (2011).

[34] G. Cohen, E. Gull, D. R. Reichman, A. J. Millis, and E. Rabani, Numerically exact long-time magnetization dynamics at the nonequilibrium Kondo crossover of the Anderson impurity model, Phys. Rev. B **87**, 195108 (2013).

[35] Y. Ashida, T. Shi, M. C. Bañuls, J. I. Cirac, and E. Demler, Solving Quantum Impurity Problems in and out of Equilibrium with the Variational Approach, Phys. Rev. Lett. **121**, 026805 (2018).

[36] T. Shi, E. Demler, and J. Ignacio Cirac, Variational study of fermionic and bosonic systems with non-Gaussian states: Theory and applications, Ann. Phys. **390**, 245 (2018).

[37] G. Cohen, E. Gull, D. R. Reichman, and A. J. Millis, Taming the Dynamical Sign Problem in Real-Time Evolution of Quantum Many-Body Problems, Phys. Rev. Lett. **115**, 266802 (2015).

[38] C. Bertrand, S. Florens, O. Parcollet, and X. Waintal, Reconstructing Nonequilibrium Regimes of Quantum Many-Body Systems from the Analytical Structure of Perturbative Expansions, Phys. Rev. X **9**, 041008 (2019).

[39] M. Maček, P. T. Dumitrescu, C. Bertrand, B. Triggs, O. Parcollet, and X. Waintal, Quantum Quasi-Monte Carlo Technique for Many-Body Perturbative Expansions, Phys. Rev. Lett. **125**, 047702 (2020).

[40] J. Thoenniss, A. Lerose, and D. A. Abanin, Nonequilibrium quantum impurity problems via matrix-product states in the temporal domain, Phys. Rev. B **107**, 195101 (2023).

[41] M. C. Bañuls, M. B. Hastings, F. Verstraete, and J. I. Cirac, Matrix Product States for Dynamical Simulation of Infinite Chains, Phys. Rev. Lett. **102**, 240603 (2009).

[42] Y.-K. Huang, P. Chen, Y.-J. Kao, and T. Xiang, Long-time dynamics of quantum chains: Transfer-matrix renormalization group and entanglement of the maximal eigenvector, Phys. Rev. B **89**, 201102(R) (2014).

[43] A. Lerose, M. Sonner, and D. A. Abanin, Influence Matrix Approach to Many-Body Floquet Dynamics, Phys. Rev. X **11**, 021040 (2021).

[44] A. Lerose, M. Sonner, and D. A. Abanin, Scaling of temporal entanglement in proximity to integrability, Phys. Rev. B **104**, 035137 (2021).

[45] E. Ye and G. K.-L. Chan, Constructing tensor network influence functionals for general quantum dynamics, J. Chem. Phys. **155**, 044104 (2021).

[46] M. Sonner, A. Lerose, and D. A. Abanin, Influence functional of many-body systems: Temporal entanglement and matrix-product state representation, Ann. Phys. **435**, 168677 (2021).

[47] M. Sonner, A. Lerose, and D. A. Abanin, Characterizing many-body localization via exact disorder-averaged quantum noise, Phys. Rev. B **105**, L020203 (2022).

[48] L. Piroli, B. Bertini, J. I. Cirac, and T. Prosen, Exact dynamics in dual-unitary quantum circuits, Phys. Rev. B **101**, 094304 (2020).

[49] K. Klobas, B. Bertini, and L. Piroli, Exact Thermalization Dynamics in the "Rule 54" Quantum Cellular Automaton, Phys. Rev. Lett. **126**, 160602 (2021).

[50] G. Giudice, G. Giudici, M. Sonner, J. Thoenniss, A. Lerose, D. A. Abanin, and L. Piroli, Temporal Entanglement, Quasiparticles, and the Role of Interactions, Phys. Rev. Lett. **128**, 220401 (2022).

[51] A. Lerose, M. Sonner, and D. A. Abanin, Overcoming the entanglement barrier in quantum many-body dynamics via space-time duality, Phys. Rev. B **107**, L060305 (2023).

[52] M. Frías-Pérez and M. C. Banuls, Light cone tensor network and time evolution, Phys. Rev. B **106**, 115117 (2022).

[53] A. Strathearn, P. Kirton, D. Kilda, J. Keeling, and B. W. Lovett, Efficient non-Markovian quantum dynamics using time-evolving matrix product operators, Nat. Commun. **9**, 3322 (2018).

[54] A. Bose and P. L. Walters, A tensor network representation of path integrals: Implementation and analysis, arXiv:2106.12523.

[55] R. P Feynman and F. Vernon, The theory of a general quantum system interacting with a linear dissipative system, Ann. Phys. **24**, 118 (1963).

[56] S. Bravyi and D. Gosset, Complexity of quantum impurity problems, Commun. Math. Phys. **356**, 451 (2017).

[57] M. Debertolis, S. Florens, and I. Snyman, Few-body nature of Kondo correlated ground states, Phys. Rev. B **103**, 235166 (2021).

[58] See Supplemental Material at http://link.aps.org/supplemental/10.1103/PhysRevB.107.L201115 for detailed derivations of the formulas used in the main text, as well as details of the matrix-product state algorithms, which includes Refs. [69,70].

[59] These include a partial "particle-hole transformation," corresponding to a swap of variables $\bar{\eta} \leftrightarrow \eta$.

[60] M. T. Fishman and S. R. White, Compression of correlation matrices and an efficient method for forming matrix product states of fermionic Gaussian states, Phys. Rev. B **92**, 075132 (2015).

[61] N. Schuch and B. Bauer, Matrix product state algorithms for Gaussian fermionic states, Phys. Rev. B **100**, 245121 (2019).

[62] M. Medvedyeva, A. Hoffmann, and S. Kehrein, Spatiotemporal buildup of the Kondo screening cloud, Phys. Rev. B **88**, 094306 (2013).

[63] T. L. Schmidt, P. Werner, L. Mühlbacher, and A. Komnik, Transient dynamics of the Anderson impurity model out of equilibrium, Phys. Rev. B **78**, 235110 (2008).

[64] P. Werner, T. Oka, M. Eckstein, and A. J. Millis, Weak-coupling quantum Monte Carlo calculations on the Keldysh contour: Theory and application to the current-voltage characteristics of the Anderson model, Phys. Rev. B **81**, 035108 (2010).

[65] D. M. Fugger, A. Dorda, F. Schwarz, J. von Delft, and E. Arrigoni, Nonequilibrium Kondo effect in a magnetic field: auxiliary master equation approach, New J. Phys. **20**, 013030 (2018).

[66] The choice of an environment defined by unitary evolution allows us to avoid errors associated with time discretization of a predefined spectral density $\Gamma(\omega)$.

[67] N. Ng, G. Park, A. J. Millis, G. K.-L. Chan, and D. R. Reichman, Real-time evolution of Anderson impurity models via tensor network influence functionals, Phys. Rev. B **107**, 125103 (2023).

[68] 10.26037/yareta:7uzfmzctave7nkyczbmccsr2fi.

[69] M. M. Wilde, *Quantum Information Theory* (Cambridge University Press, Cambridge, UK, 2013).

[70] In a strict sense, $\{A_\sigma(m)\}_{m=1}^{M}$ are not superoperators as their bond dimension (and thus the equivalent of the environment operator space) is not guaranteed to be a square integer, and completely positive trace-preserving (CPTP) property is not enforced. Furthermore, this property would require to fix the gauge freedom of the MPS.